

# Solvent-dependent selective cation exchange in anionic frameworks based on cobalt(II) and triphenylamine linkers: reactor-dependent synthesis and sorption properties

Oluseun Akintola, David Hornig, Axel Buchholz, Helmar Görls, Winfried Plass

## Supplementary Information

### Contents

|     |   |    |
|-----|---|----|
| 1   | Reactor vessels   | 3  |
| 2   | Analytical data for cation-exchanged samples              | 4  |
| 2.1 | Exchange with lithium ions                                | 4  |
| 2.2 | Exchange with europium(III) ions                          | 5  |
| 3   | Additional structure information for JUMP-2               | 6  |
| 4   | Topological analysis                                      | 10 |
| 4.1 | Topological analysis for JUMP-2                           | 10 |
| 4.2 | Topological analysis for MIL-144                          | 10 |
| 4.3 | Tiling of MIL-144   | 11 |
| 5   | XRPD patterns of as-synthesized samples                   | 12 |
| 6   | TGA profiles  | 13 |
| 7   | Alternating current (ac) magnetic measurements for JUMP-2 | 14 |
| 8   | Magnetization data for MIL-144                            | 18 |
| 9   | XRPD patterns for cation exchanged samples                | 19 |

|      |   |    |
|------|---|----|
| 10   | Fluorescence monitored europium(III) exchange | 20 |
| 11   | Sorption data                                 | 21 |
| 12   | Quantum mechanical calculations               | 22 |
| 12.1 | Computational details. . . . .                | 22 |
| 12.2 | Magnetic anisotropy for JUMP-2 . . . . .      | 22 |
|      | Bibliography                                  | 27 |

## 1 Reactor vessels



**Fig. S1:** Reactor vessels utilized in MOF syntheses: (Left) 110 mL Perkin Elmer acid digestion bomb for MIL-144. (Right) 23 mL Parr acid digestion bomb for JUMP-2.

## 2 Analytical data for cation-exchanged samples

### 2.1 Exchange with lithium ions

JUMP-2(Li)E

*Analytical Data for  $[(Me_2NH_2)Li[Co(ntb)Cl] \cdot C_2H_5OH \cdot 1.5 DMF]_n$*

Anal. Calcd for  $C_{29.5}H_{36.5}ClCoLiN_{3.5}O_{8.5}$  ( $677.45\text{ g mol}^{-1}$ ):

C 52.30, H 5.43, N 7.24 %. Found: C 52.10, H 5.35, N 7.39 %.

Selected IR (ATR,  $\text{cm}^{-1}$ ): 1651w, 1591s, 1506m, 1370s, 1313s, 1271s, 1174s, 1103m, 1045m.

JUMP-2(Li)D

*Analytical Data for  $[(Me_2NH_2)Li[Co(ntb)Cl] \cdot C_2H_5OH \cdot DMF \cdot H_2O]_n$*

Anal. Calcd for  $C_{28}H_{35}ClCoLiN_3O_9$  ( $658.92\text{ g mol}^{-1}$ ):

C 51.04, H 5.35, N 6.38 %. Found: C 51.10, H 5.61, N 6.17 %.

Selected IR (ATR,  $\text{cm}^{-1}$ ): 1652w, 1591s, 1506m, 1372s, 1313s, 1270s, 1173s, 1088m, 1045m.

MIL-144(Li)E

*Analytical Data for  $[Li_2[Co_5(ntb)_4(H_2O)_3(C_2H_5OH)] \cdot 17H_2O]_n$*

Anal. Calcd for  $C_{86}H_{94}Co_5Li_2N_4O_{45}$  ( $2212.21\text{ g mol}^{-1}$ ):

C 46.69, H 4.28, N 2.53 %. Found: C 46.67, H 4.20, N 2.36 %.

Selected IR (ATR,  $\text{cm}^{-1}$ ): 1589s, 1535m, 1506m, 1378vs, 1313s, 1270s, 1176s, 1087m, 1045m.

MIL-144(Li)D

*Analytical Data for  $[(Me_2NH_2)Li[Co_5(ntb)_4(H_2O)_3(C_2H_5OH)]_n \cdot 3C_2H_5OH \cdot 2H_2O]$*

Anal. Calcd for  $C_{94}H_{90}Co_5LiN_5O_{33}$  ( $2119.34\text{ g mol}^{-1}$ ):

C 53.27, H 4.28, N 3.30 %. Found: C 53.18, H 4.41, N 3.20 %.

Selected IR (ATR,  $\text{cm}^{-1}$ ): 1589s, 1536m, 1505m, 1376vs, 1312s, 1269s, 1175s, 1088m, 1043m.

## 2.2 Exchange with europium(III) ions

JUMP-2(Eu)E

*Analytical Data for  $[(MeNH_2)_3Eu([Co(ntb)Cl]_3)_3 \cdot 3C_2H_5OH \cdot 6DMF$*

Anal. Calcd for  $C_{93}H_{120}Cl_3Co_3EuN_{12}O_{27}$  ( $2273.13\text{ g mol}^{-1}$ ):

C 49.14, H 5.32, N 7.39 %. Found: C 49.52, H 5.03, N 7.22 %.

Selected IR (ATR,  $\text{cm}^{-1}$ ): 1653w, 1594s, 1505m, 1367s, 1313s, 1268s, 1170s, 1103m.

JUMP-2(Eu)D

*Analytical Data for  $[Eu_2([Co(ntb)Cl]_3)_3 \cdot 9C_2H_5OH \cdot 3DMF$*

Anal. Calcd for  $C_{90}H_{111}Cl_3Co_3Eu_2N_6O_{30}$  ( $2343.95\text{ g mol}^{-1}$ ):

C 46.12, H 4.77, N 3.59 %. Found: C 46.08, H 4.91, N 3.77 %.

Selected IR (ATR,  $\text{cm}^{-1}$ ): 1591s, 1535m, 1506m, 1376vs, 1313s, 1271s, 1174s, 1088m, 1043s.

MIL-144(Eu)E

*Analytical Data for  $[(Me_2NH_2)_3Eu[Co_5(ntb)_4(H_2O)_3(C_2H_5OH)]_3 \cdot 54H_2O \cdot 18C_2H_5OH$*

Anal. Calcd for  $C_{300}H_{420}Co_{15}EuN_{15}O_{156}$  ( $7768.51\text{ g mol}^{-1}$ ):

C 46.38, H 5.45, N 2.70 %. Found: C 46.37, H 5.68, N 2.44 %.

Selected IR (ATR,  $\text{cm}^{-1}$ ): 1589s, 1529m, 1504m, 1382vs, 1312s, 1270s, 1175s, 1086m, 1042s.

MIL-144(Eu)D

*Analytical Data for  $[(Me_2NH_2)_3Eu[Co_5(ntb)_4(H_2O)_3(C_2H_5OH)]_3 \cdot 42H_2O \cdot 18C_2H_5OH$*

Anal. Calcd for  $C_{300}H_{396}Co_{15}EuN_{15}O_{144}$  ( $7552.33\text{ g mol}^{-1}$ ):

C 47.71, H 5.29, N 2.78 %. Found: C 47.75, H 5.20, N 2.94 %.

Selected IR (ATR,  $\text{cm}^{-1}$ ): 1590s, 1535m, 1505m, 1382vs, 1312s, 1271s, 1175s, 1087m, 1043s.

### 3 Additional structure information for JUMP-2

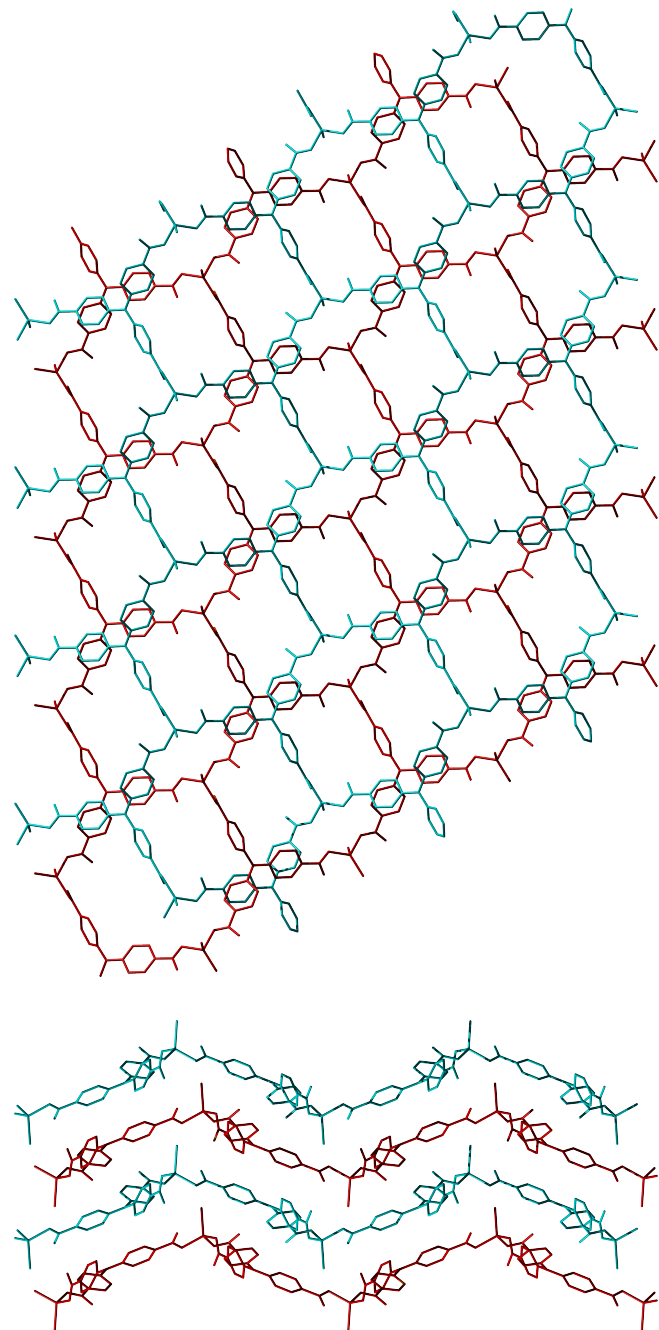


**Fig. S2:** 2D layered arrangement of the anionic framework in JUMP-2 showing the staggered arrangement: (Top) View along the [010] direction. (Bottom) Side view along the [̄100] direction.

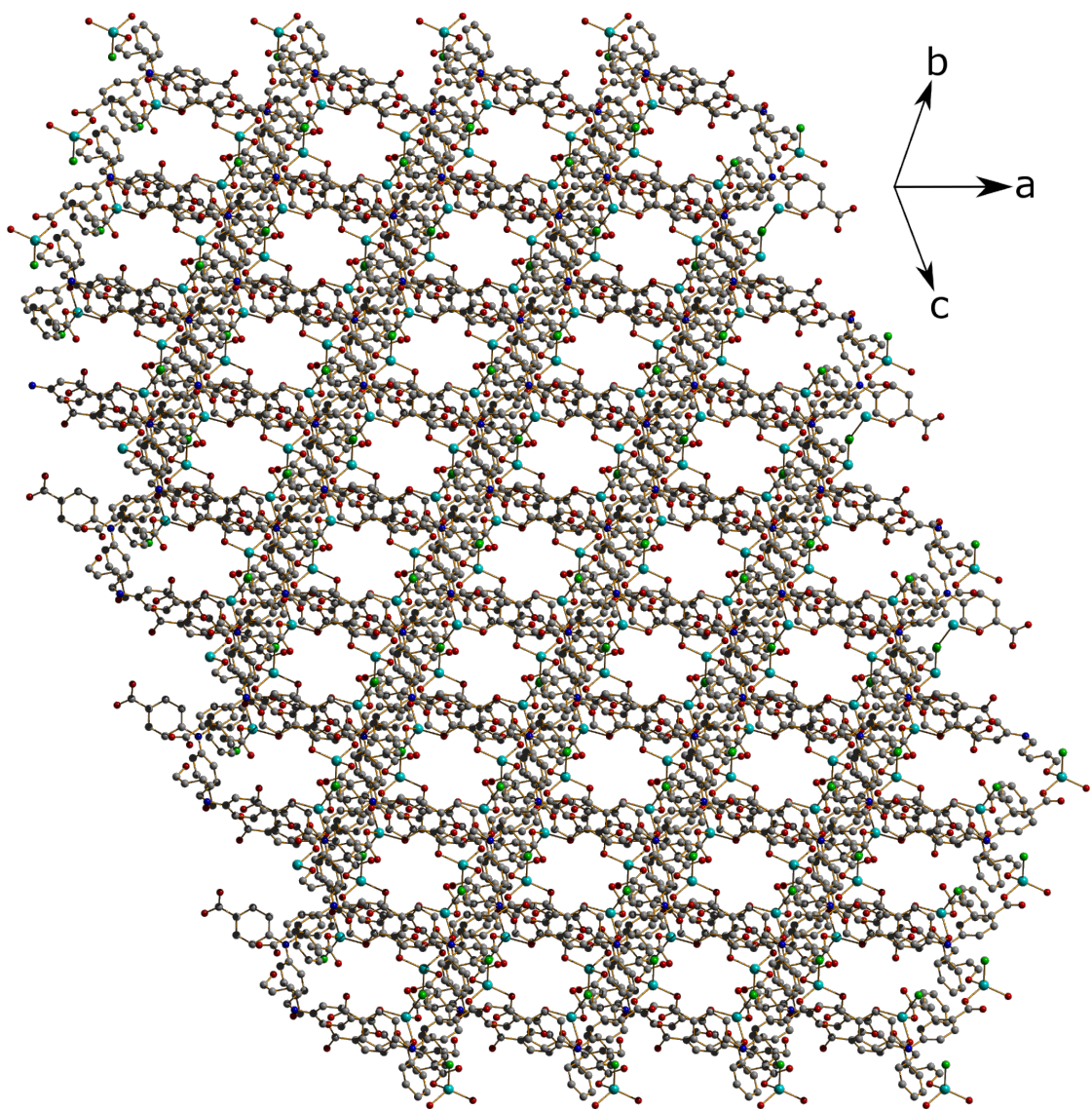


**Fig. S3:** 1D channels in the anionic framework of JUMP-2 viewed along  $[12\bar{1}]$  direction.

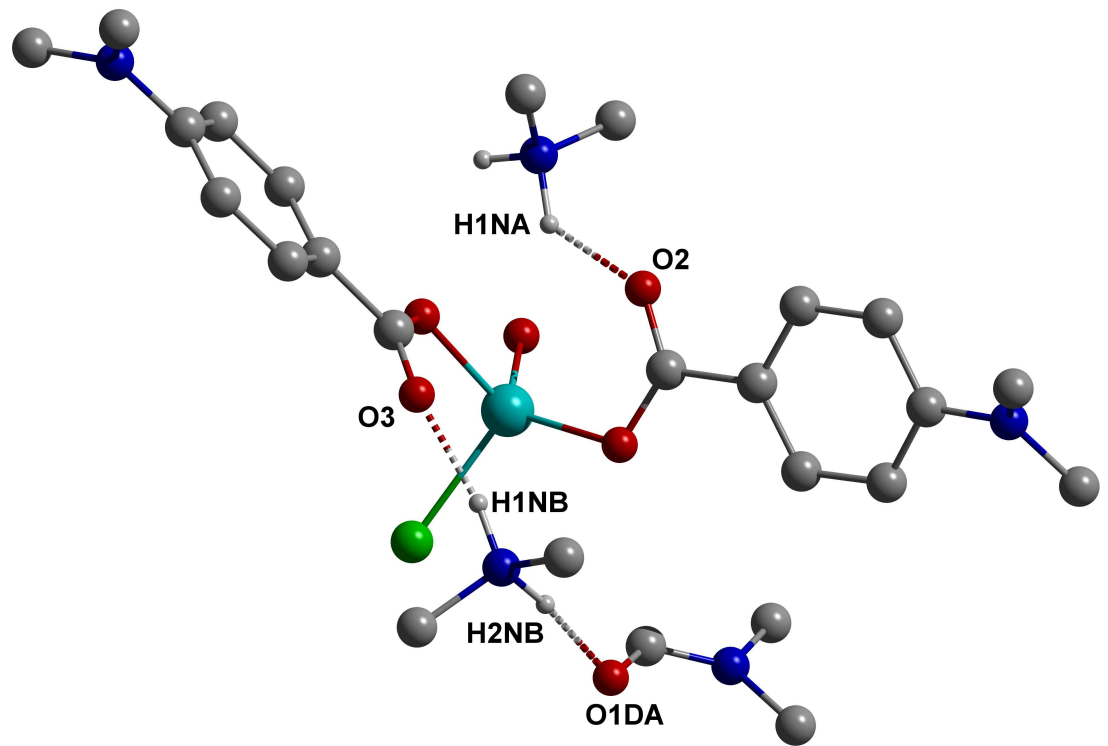


**Fig. S4:** Representation of the hydrogen bonding interactions for a cutout of the anionic framework of JUMP-2. Pertinent data:  $O_2 \cdots N_1 EA$  271.7(5),  $O_3 \cdots N_1 EB$  271.1(5),  $O_1 DA \cdots N_1 EB$  277.0(9) pm.

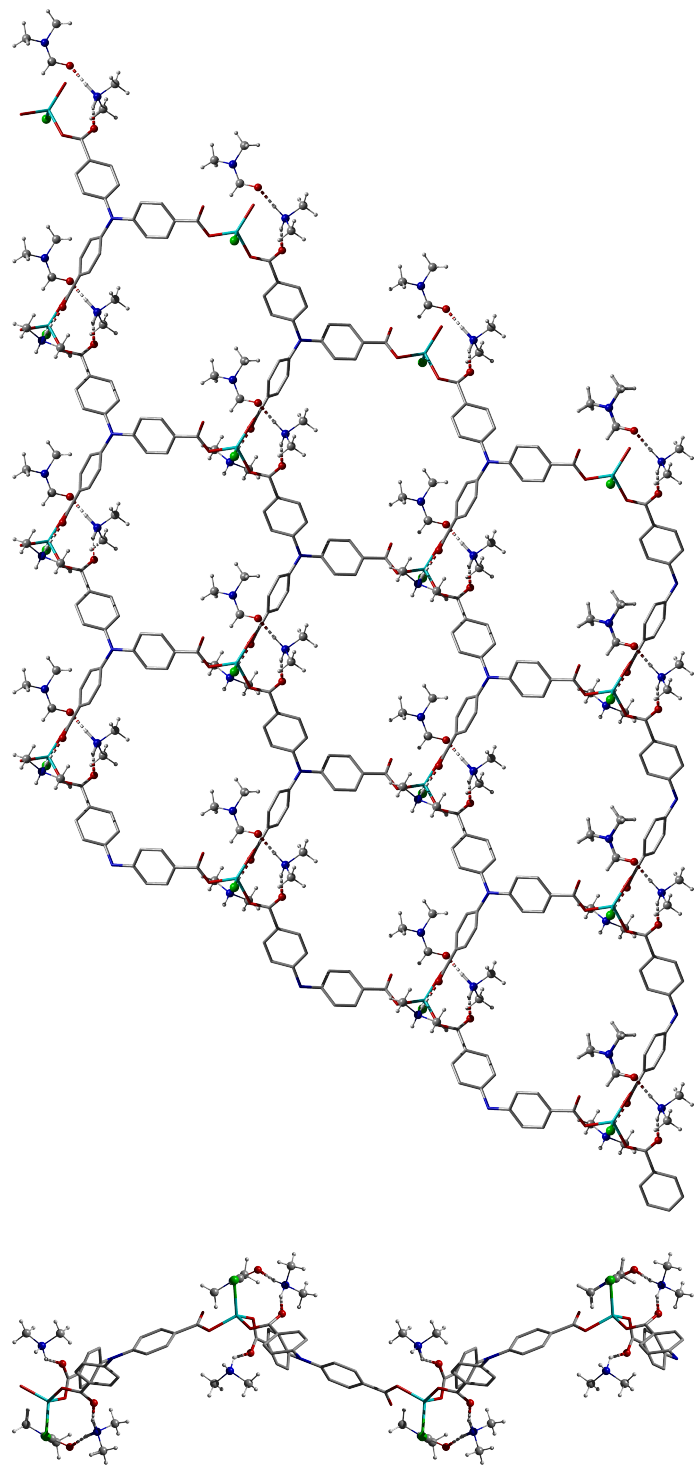


**Fig. S5:** Representation of the hydrogen bonding around the 2D layers in JUMP-2 viewed along [010] direction: (Top) View along the [010] direction. (Bottom) Side view of one layer along the [100] direction.

## 4 Topological analysis

### 4.1 Topological analysis for JUMP-2

Ideal space group is  $P6mm$ .

**Table S1:** Coordination sequences for JUMP-2 (topological density  $TD_{10} = 166$ )

| Vertex | $CS_1$ | $CS_2$ | $CS_3$ | $CS_4$ | $CS_5$ | $CS_6$ | $CS_7$ | $CS_8$ | $CS_9$ | $CS_{10}$ |
|--------|--------|--------|--------|--------|--------|--------|--------|--------|--------|-----------|
| V1     | 3      | 6      | 9      | 12     | 15     | 18     | 21     | 24     | 27     | 30        |
| V2     | 3      | 6      | 9      | 12     | 15     | 18     | 21     | 24     | 27     | 30        |

**Table S2:** Vertex Symbols for JUMP-2

| Vertex | Vertex symbol | Extended Point Symbol |
|--------|---------------|-----------------------|
| V1     | $[6^3]$       | $[6.6.6]$             |
| V2     | $[6^3]$       | $[6.6.6]$             |

### 4.2 Topological analysis for MIL-144

Ideal space group:  $R\bar{3}c$ .

**Table S3:** Coordination sequences for MIL-144 (topological density  $TD_{10} = 1192$ )

| Vertex | $CS_1$ | $CS_2$ | $CS_3$ | $CS_4$ | $CS_5$ | $CS_6$ | $CS_7$ | $CS_8$ | $CS_9$ | $CS_{10}$ |
|--------|--------|--------|--------|--------|--------|--------|--------|--------|--------|-----------|
| V1     | 3      | 13     | 16     | 52     | 45     | 134    | 103    | 257    | 171    | 418       |
| V2     | 6      | 8      | 32     | 30     | 90     | 76     | 206    | 140    | 342    | 218       |

**Table S4:** Vertex Symbols for MIL-144

| Vertex | Vertex symbol      | Extended Point Symbol                           |
|--------|--------------------|---|
| V1     | $[4^2.6]$          | $[4.4.6]$                                       |
| V2     | $[4^4.6^2.8^8.10]$ | $[4.4.4.4.6.6.8_2.8_3.8_4.8_7.8_7.8_7.10_{14}]$ |

### 4.3 Tiling of MIL-144

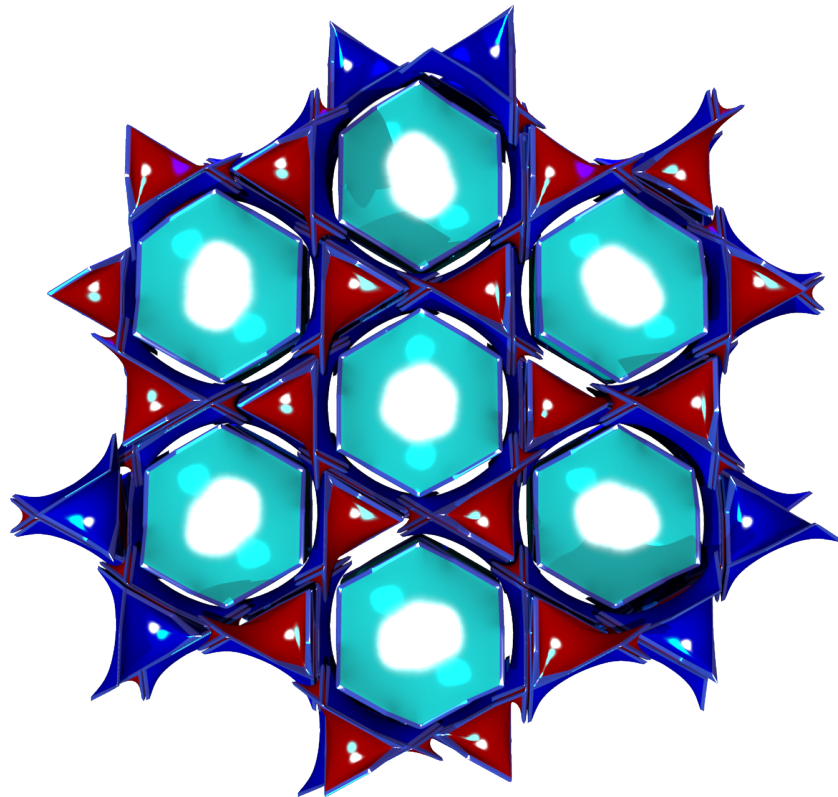


**Fig. S6:** Tiling of MIL-144 viewed along [001]. Tiles:  $3[4^2 \cdot 8^2 \cdot] + 3[4 \cdot 8^3] + [4^3 \cdot 8^3 \cdot 12^2]$ .  
Transitivity: [2353].

## 5 XRPD patterns of as-synthesized samples

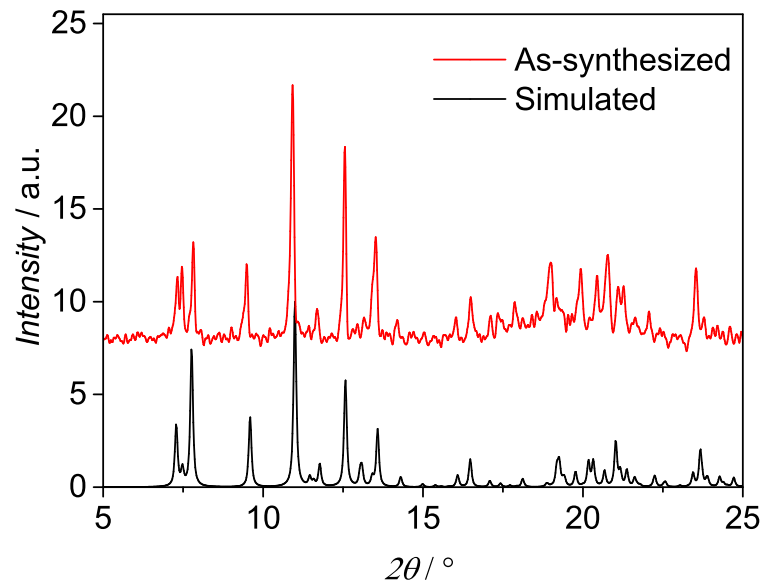


**Fig. S7:** XRPD pattern for JUMP-2.

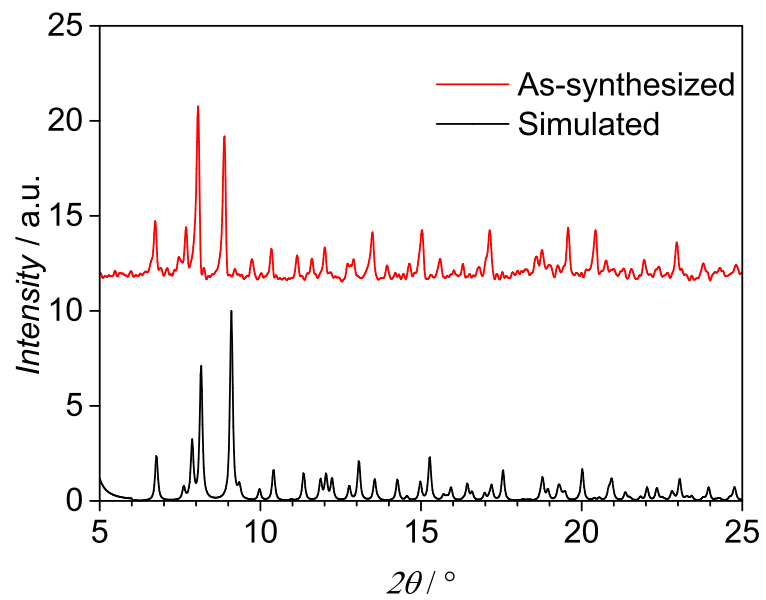


**Fig. S8:** XRPD pattern for MIL-144.

## 6 TGA profiles

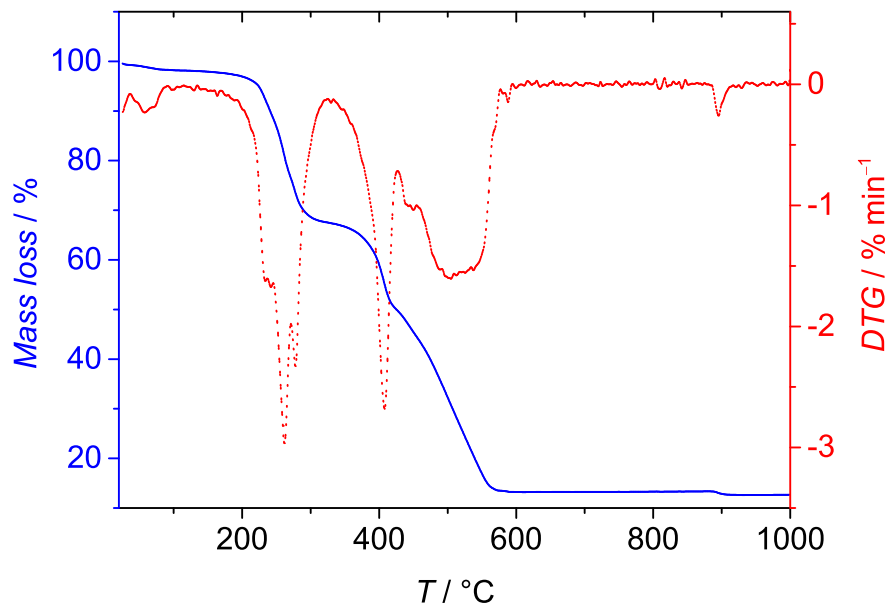


**Fig. S9:** TGA profile for JUMP-2.

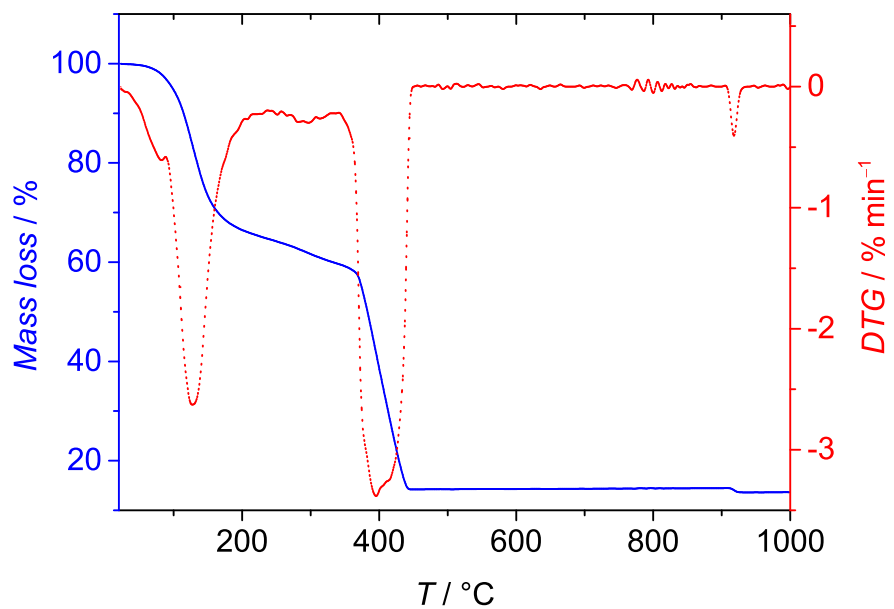


**Fig. S10:** TGA profile for MIL-144.

## 7 Alternating current (ac) magnetic measurements for JUMP-2

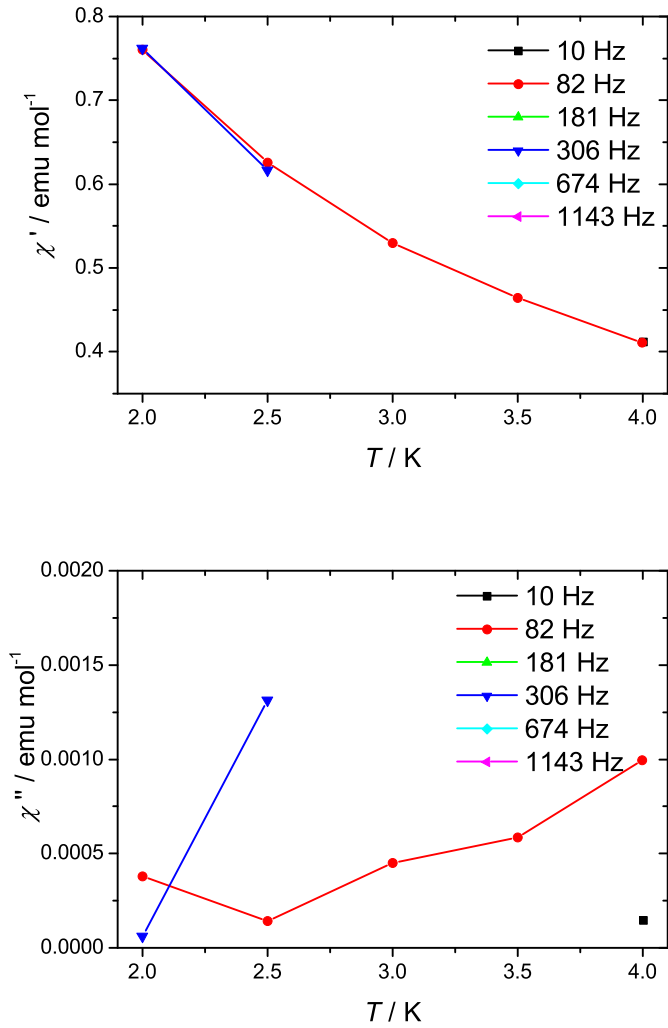


**Fig. S11:** Temperature dependence of the real (top) and imaginary (bottom) part of the susceptibility for JUMP-2 at a dc field of 0 Oe.

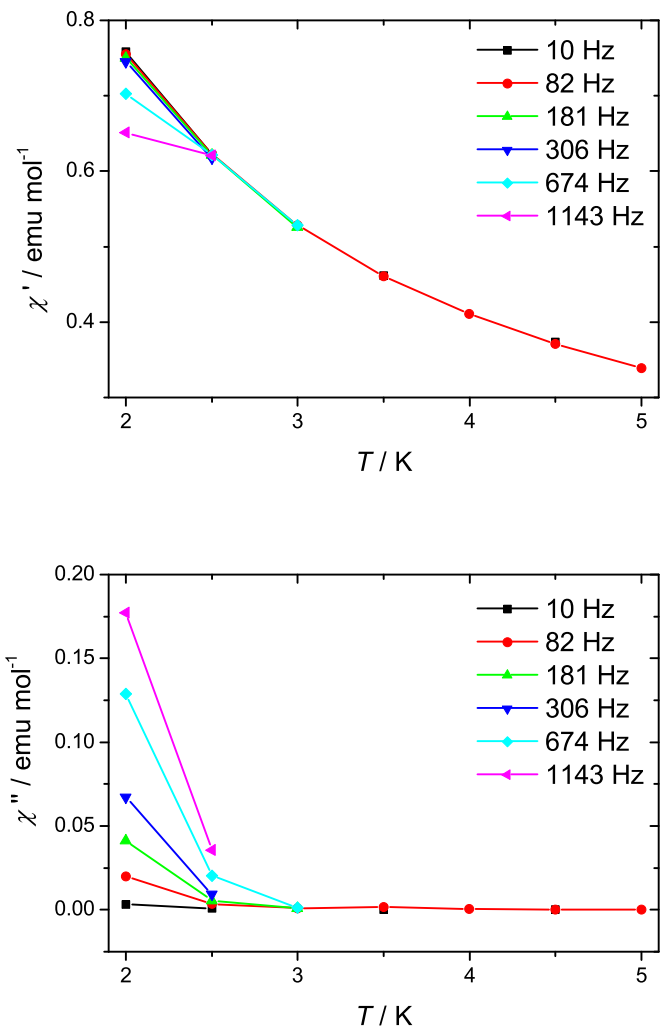


**Fig. S12:** Temperature dependence of the real (top) and imaginary (bottom) part of the susceptibility for JUMP-2 at a dc filed of 400 Oe.

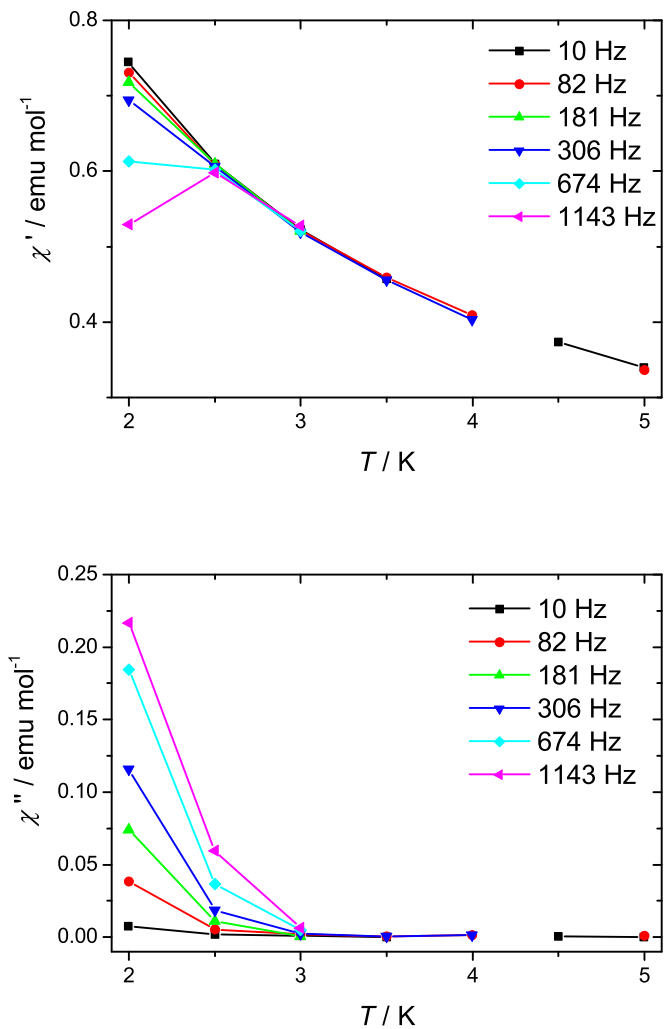


**Fig. S13:** Temperature dependence of the real (top) and imaginary (bottom) part of the susceptibility for JUMP-2 at a dc field of 1000 Oe.

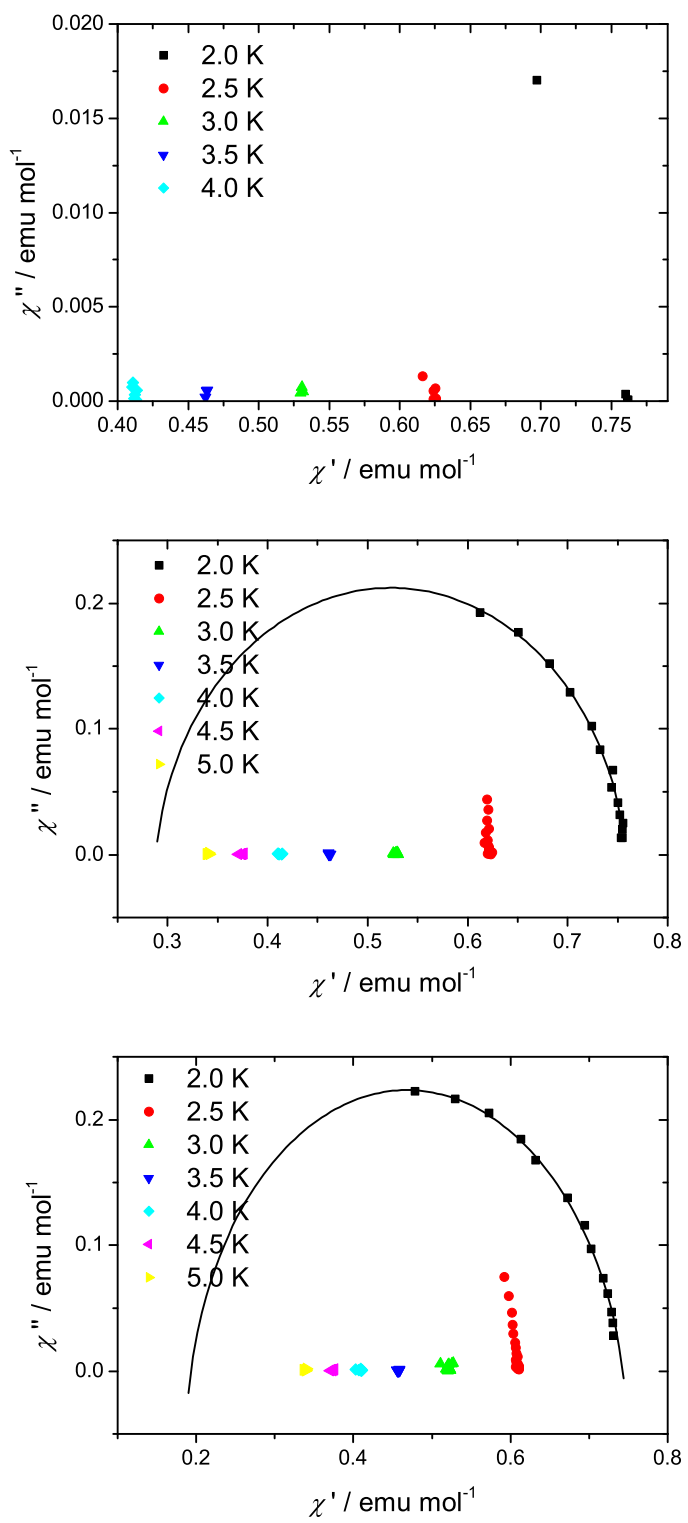


**Fig. S14:** Cole-cole plots for JUMP-2 at 0 Oe (top) 400 Oe (middle), and 1000 Oe (bottom).

## 8 Magnetization data for MIL-144

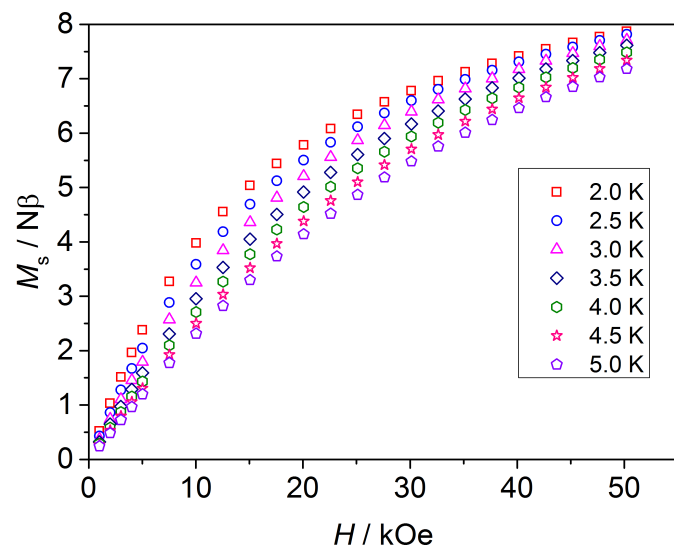


**Fig. S15:** Temperature- and field-dependent magnetization data for MIL-144.

## 9 XRPD patterns for cation exchanged samples

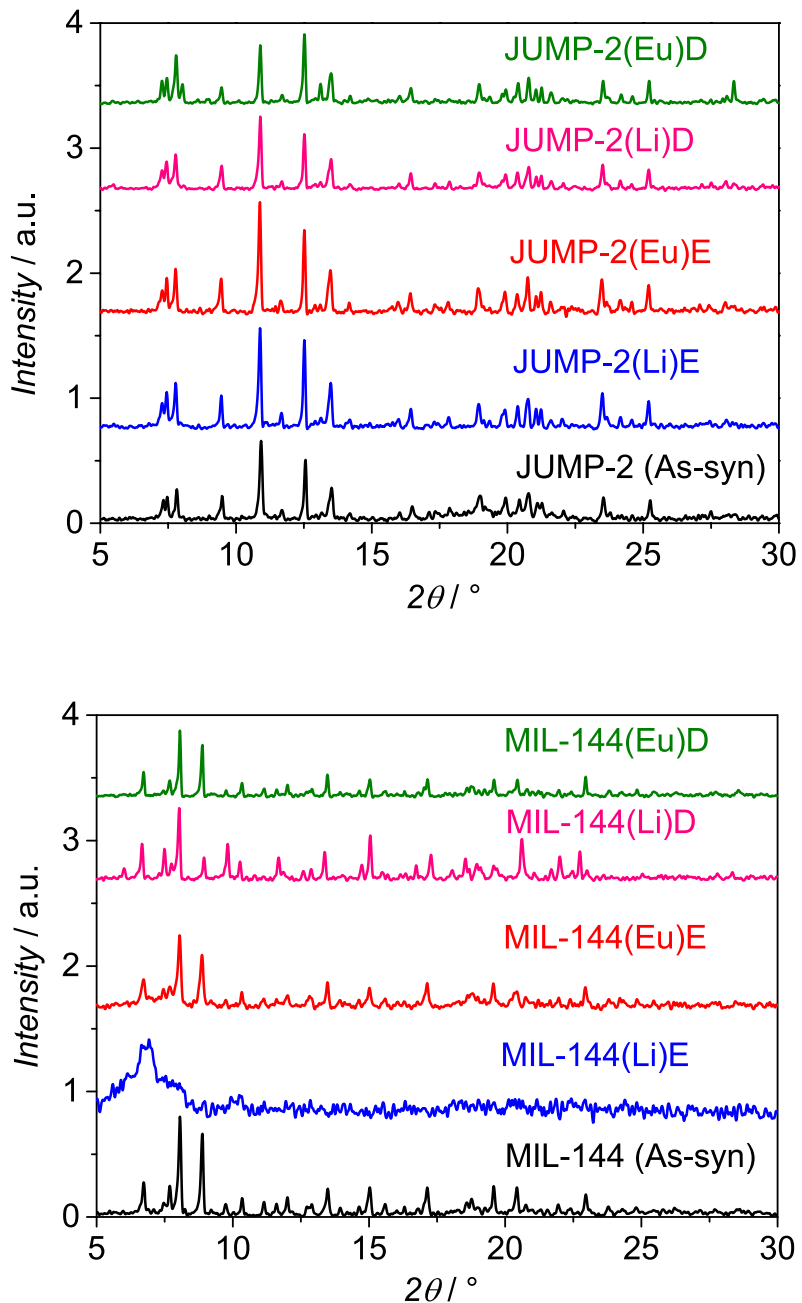


**Fig. S16:** XRPD patterns for the as-synthesized and cation exchanged samples of both JUMP-2 (top) and MIL-144 (bottom).

## 10 Fluorescence monitored europium(III) exchange

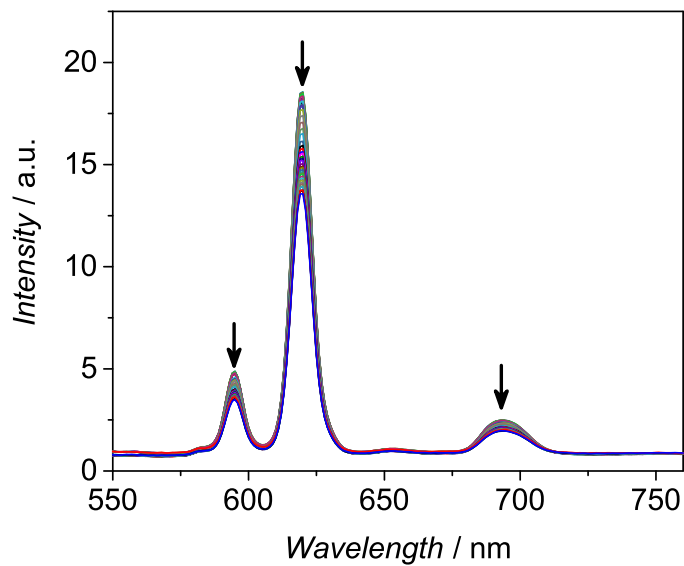
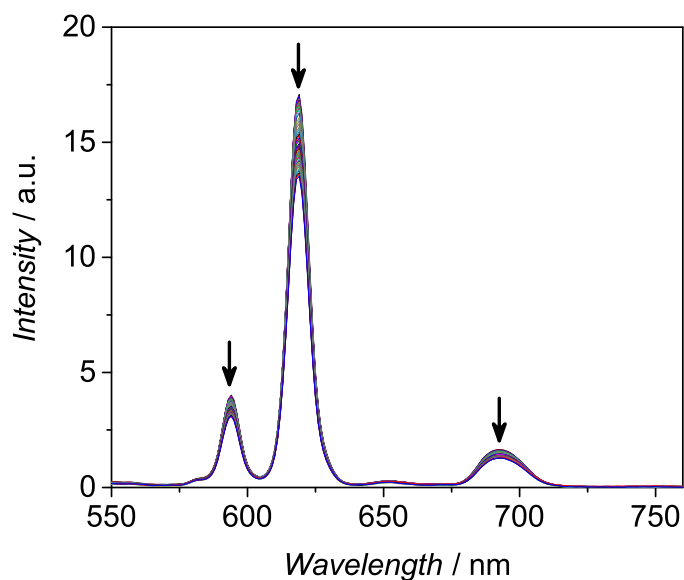


**Fig. S17:** Cation exchange experiment for JUMP-2 (top) and MIL-144 (bottom) with europium(III) nitrate in ethanol. Fluorescence spectra depicted were measured in time intervals of 1 h over a period of 48 h at an excitation wave length of 395 nm.

## 11 Sorption data

**Table S5:** Consistency criteria derived from measured BET Data for the as-synthesized and lithium ion exchanges samples of JUMP-2 and MIL-144 after application of supercritical drying with CO<sub>2</sub>

|                             | P/P <sub>o</sub> range | C    | V <sub>m</sub> [cm <sup>3</sup> /g] | 1/√C + 1 | P/P <sub>o</sub> (V <sub>m</sub> ) | a(BET) [m <sup>2</sup> /g] | R     |
|-----------------------------|------------------------|------|-------------------------------------|----------|------------------------------------|----------------------------|-------|
| JUMP-2 <sup>scd</sup>       | 0.13 - 0.28            | 7    | 2.99                                | 0.27     | 0.27                               | 13                         | 0.999 |
| JUMP-2(Li)D <sup>scd</sup>  | 0.13 - 0.30            | 7    | 5.40                                | 0.27     | 0.27                               | 24                         | 0.997 |
| JUMP-2(Eu)D <sup>scd</sup>  | 0.05 - 0.15            | 147  | 49.64                               | 0.08     | 0.08                               | 216                        | 0.999 |
| MIL-144 <sup>scd</sup>      | 0.13 - 0.28            | 16   | 4.84                                | 0.20     | 0.20                               | 21                         | 0.999 |
| MIL-144(Li)E <sup>scd</sup> | 0.005 - 0.08           | 1491 | 86.96                               | 0.03     | 0.03                               | 380                        | 0.999 |
| MIL-144(Eu)E <sup>scd</sup> | 0.005 - 0.08           | 1911 | 44.43                               | 0.02     | 0.02                               | 194                        | 0.999 |

## 12 Quantum mechanical calculations

### 12.1 Computational details.

For all atoms the triple- $\zeta$  basis set def2-TZPV proposed by Ahlrichs et al.<sup>1</sup> was used. Calculations were performed for molecular models with the position of the non-hydrogen atoms taken from the crystal structures and the positions of the hydrogen atoms were optimized. These optimizations were carried out using the B88 exchange functional<sup>2</sup> and the correlation functionals VWN(V)<sup>3</sup> and P86.<sup>4</sup> The geometry optimizations were accelerated further by employing the resolution of identity approximation. The CASSCF,<sup>5</sup> CASPT2,<sup>6</sup> and RASSI-SO<sup>7</sup> calculations were carried out for the aforementioned model systems with optimized hydrogen atoms employing the MOLCAS 7.8 package.<sup>8</sup> ANO-RCC type basis sets<sup>9</sup> were used for all atoms (contractions: Co–6s5p4d2f1g, coordinating O and N–4s3p2d1f, peripheral N and C–3s2p, H–2s). To save computational time and disk space, the Choleski decomposition was used. Calculations for cobalt(II) involved a (7,10) active space with a double d-set of orbitals. 10 quartet states and 40 doublet states were calculated within the CASSCF procedure to account for all states arising from the d<sup>7</sup> configuration. CASPT2 calculations were done on all quartet states and on the 12 lowest doublet states. Otherwise, intruder states were regularly encountered. RASSI-SO calculations were performed on the CASPT2 wave functions for the states calculated. Calculations of the magnetic properties for mononuclear complexes were performed using the SINGLE\_ANISO module.<sup>10</sup>

### 12.2 Magnetic anisotropy for JUMP-2

Quantum mechanical investigations on the electronic structure of the single cobalt(II) ions in JUMP-2 were performed by utilizing multiconfigurational wave function theory within the CASSCF/CASPT2/RASSI-SO methodology. For these calculations the approximation of the cobalt(II) environment is based on a cutout of the infinite two-dimensional layer from the crystal structure of JUMP-2 which is depicted in Figure S18. The CASSCF and CASPT2 energies summarized in Table S6 and their comparison shows only moderate changes upon inclusion of dynamic correlation. The ground state is separated by 3260 cm<sup>-1</sup> from the first excited spin-free state and resembles the expected  $A_2$  ground term, while the excited  $T_2$  and  $T_1$  term are split due to the deviation from  $T_d$  symmetry. Doublet states are found to follow above 16000 cm<sup>-1</sup>, which confirms the high-spin ground state suggested by experiment. Calculations of the spin-orbit states furthermore show a rather weak mixing of the spin-free ground state with excited states, with a leading weight of over 0.97. This also leads to a small energy gap of 25 cm<sup>-1</sup> with respect to the first excited Kramers doublet (KD). In addition the  $g$  elements obtained for the ground state KD show considerable rhombic

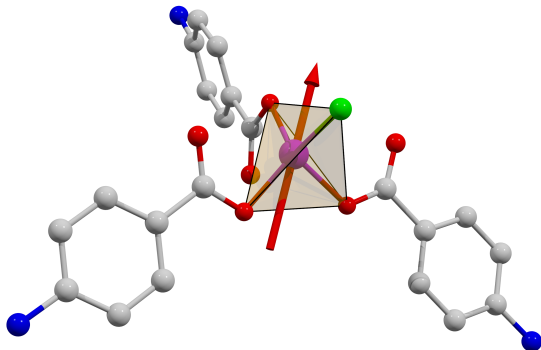


**Fig. S18:** Representation of the main anisotropy axis of the ground state Kramers doublet derived from multiconfigurational calculations on JUMP-2 for the depicted model structure. Hydrogen atoms are omitted for clarity.

components of over 0.8 (Table S7). Zero-field splitting (ZFS) parameters calculated with the SINGLE\_ANISO program reveal easy-axis anisotropy ( $D = -11.9 \text{ cm}^{-1}$ ), however, with a significant rhombic distortion of  $E = -1.7 \text{ cm}^{-1}$ . In fact, these parameters can reproduce the experimental magnetization data as shown in Figure S19 and are consistent with the presence of efficient relaxation processes already seen from the experimental absence of a relevant single-ion magnet behavior for JUMP-2.

**Table S6:** Spin-free CASSCF and CASPT2 energies ( $\text{cm}^{-1}$ ) of the quartet and doublet states for JUMP-2. To avoid intruder states, only the 12 lowest doublet states were included in the CASPT2 calculations

|                | CASSCF | CASPT2 |
|----------------|--------|--------|
| quartet states | 0      | 0      |
|                | 2853   | 3260   |
|                | 3841   | 4018   |
|                | 4536   | 4419   |
|                | 5254   | 5621   |
|                | 7303   | 8093   |
|                | 7925   | 8905   |
|                | 20589  | 17524  |
|                | 21853  | 18829  |
|                | 22544  | 19663  |
| doublet states | 19376  | 16914  |
|                | 19664  | 17202  |
|                | 20149  | 17637  |
|                | 20215  | 17661  |
|                | 20567  | 18121  |
|                | 21277  | 18953  |
|                | 22204  | 19849  |
|                | 22492  | 20424  |
|                | 22985  | 20823  |
|                | 25420  | 22817  |
|                | 25774  | 23198  |
|                | 26152  | 23758  |
| ...            |        |        |

**Table S7:** Energies and  $g$  values of the lowest KDs of JUMP-2 calculated with the CASPT2/RASSI-SO procedure

| KD |       | $E$ ( $\text{cm}^{-1}$ ) | $g$ value |
|----|-------|--------------------------|-----------|
| 1  | $g_1$ |                          | 0.8605    |
|    | $g_2$ | 0                        | 1.0064    |
|    | $g_3$ |                          | 7.0316    |
| 2  | $g_1$ |                          | 2.2564    |
|    | $g_2$ | 25                       | 3.5240    |
|    | $g_3$ |                          | 5.3774    |

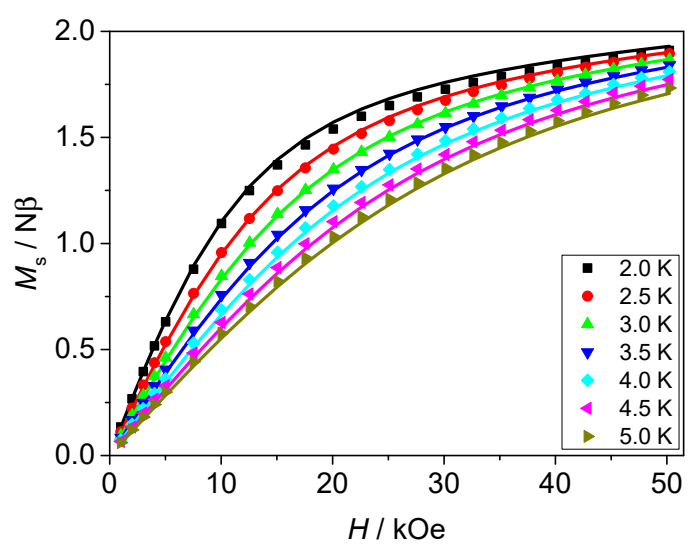


**Fig. S19:** Temperature- and field-dependent magnetization data for JUMP-2. Lines represent the simulated data based on the parameters obtained from CASPT2/RASSI-SO calculations.

## Bibliography

- [1] F. Weigend and R. Ahlrichs, *Phys. Chem. Chem. Phys.*, 2005, **7**, 3297–3305.
- [2] A. D. Becke, *Phys. Rev. A*, 1988, **38**, 3098–3100.
- [3] S. H. Vosko, L. Wilk and M. Nusair, *Can. J. Phys.*, 1980, **58**, 1200–1211.
- [4] J. P. Perdew and W. Yue, *Phys. Rev. B*, 1986, **33**, 8800–8802.
- [5] B. O. Roos, P. R. Taylor and P. E. Siegbahn, *Chem. Phys.*, 1980, **48**, 157–173.
- [6] J. Finley, P.-A. Malmqvist, B. O. Roos and L. Serrano-Andrés, *Chem. Phys. Lett.*, 1998, **288**, 299–306.
- [7] P. Å. Malmqvist, B. O. Roos and B. Schimmelpfennig, *Chem. Phys. Lett.*, 2002, **357**, 230–240.
- [8] F. Aquilante, L. De Vico, N. Ferré, G. Ghigo, P.-Å. Malmqvist, P. Neogrády, T. B. Pedersen, M. Pitoňák, M. Reiher, B. O. Roos, L. Serrano-Andrés, M. Urban, V. Veryazov and R. Lindh, *J. Comput. Chem.*, 2010, **31**, 224–247.
- [9] (a) B. O. Roos, R. Lindh, P.-Å. Malmqvist, V. Veryazov and P.-O. Widmark, *J. Phys. Chem. A*, 2004, **108**, 2851–2858; (b) B. O. Roos, R. Lindh, P.-A. Malmqvist, V. Veryazov and P.-O. Widmark, *J. Phys. Chem. A*, 2005, **109**, 6575–6579; (c) B. O. Roos, R. Lindh, P.-A. Malmqvist, V. Veryazov, P.-O. Widmark and A. C. Borin, *J. Phys. Chem. A*, 2008, **112**, 11431–11435.
- [10] L. F. Chibotaru and L. Ungur, *J. Chem. Phys.*, 2012, **137**, 064112.